Sensors & Actuators: B. Chemical 401 (2024) 135038

Contents lists available at ScienceDirect

Sensors and Actuators: B. Chemical

journal homepage: www.elsevier.com/locate/snb

Confinement of gold nanoclusters on hydroxy double salt for versatile fluorescent sensing of bio-enzymes

Mengke Wang [a], Yaqing Han [a], Rui Huang [b], Zhonghao Wang [a], Guannan Wang [c,*]

[a] College of Medical Engineering & the Key Laboratory for Medical Functional Nanomaterials, Jining Medical University, Jining 272067, PR China
[b] School of Materials Science and Engineering, Hainan University, Haikou 570228, PR China
[c] School of Pharmacy, Shenyang Medical University, Shenyang 110034, China

ARTICLE INFO

Keywords:
Fluorescence
Gold nanoclusters
Confinement effect
Hydroxy double salt
Bio-enzymes

ABSTRACT

Fluorescent gold nanoclusters (AuNCs) have generated significant research interest because of their fascinating physicochemical properties. However, their biosensing applications are limited by the relatively low quantum yield (QY). Herein, a simple confinement effect based on AuNCs as guest molecules and Zn-containing hydroxy double salt (HDS) as host material (AuNCs@HDS) was used to significantly improve the fluorescence properties of AuNCs. The QY increased from 1.24 % to 22.80 %, and the time-tedious preparation or purification procedures were avoided. Further, the validated excellent fluorescence properties of AuNCs enabled the construction of a versatile fluorescent sensing strategy for bio-enzymes for the first time. The p-nitrophenol (pNP), a product of many bio-enzymes-catalyzed hydrolyzes of pNP-substrate, can effectively quench the fluorescence of AuNCs@HDS through an inner filter effect (IFE) process. Therefore, the AuNCs@HDS successfully detected several enzymatic disease biomarkers with robust analysis capabilities by varying the pNP-substrate, including alkaline phosphatase (ALP), β-glucosidase (β-GLU) and β-galactosidase (β-GAL). This study will inspire the design of highly fluorescent AuNCs as tools for biosensing.

1. Introduction

Gold nanoclusters (AuNCs) have generated broad interest because of their fascinating physicochemical properties, such as strong photoluminescence responses, molecule-like properties, and ultrasmall sizes [1–3]. Compared with the well-developed fluorescence probes, such as organic dyes and inorganic quantum dots (QDs), AuNCs display large Stokes shift, low toxicity, and good biocompatibility [4,5]. However, the existing AuNCs exhibit a relatively low QY (usually less than 10%) because the freely rotating ligands cause excessive energy loss with nonradiative relaxation, constraining the extensive applications in imaging or labeling [6–8]. Therefore, developing new materials and strategies for constructing AuNCs with superior fluorescence performances remains challenging.

Several attempts have been made to fabricate stable and highly fluorescent AuNCs, such as ligand exchange [9], aggregation-induced emission [10,11], metal doping [12,13], and confinement strategy [14,15]. Among these methods, the confinement strategy has attracted significant interest because they endow AuNCs with strong fluorescence properties. This strategy involves restricting the free movement and improving the electron-hole pair recombination efficiency of guest fluorescent molecules under the limitation of the host materials [16]. Several host materials have been employed for confinement effect to construct highly fluorescent AuNCs. Wang's group enhanced the QY of AuNCs 6-fold by skillfully impregnating the AuNCs into a cationic polymer nanogel [16]. Yin et al. encapsulated AuNCs into the metal-organic frameworks (ZIF-8) to improve the fluorescence performance of AuNCs [17]. Despite significant QY enhancement, these strategies require tedious material synthesis or purification steps. Recently, confining nanoprobes, such as ZnS QDs [18] and CuNCs [19,20], on host materials by applying electrostatic interaction as the main binding force attracted significant attention since it enabled the simultaneous enhancement of the fluorescent emission and stability of nanoprobes in a simple non-covalent manner [21,22]. These studies inspired preparing eligible host materials that boost the fluorescence of AuNCs by the electrostatic assembly.

Hydroxy double salt (HDS), a layered metal hydroxide, has stimulated research interest with the advantages of low cost, non-toxicity, and simple preparation [23,24]. Notably, the presence of high positive charge density and rich lone pair electrons make it act as a dispersion

* Corresponding author.
E-mail address: chemwangguannan@gmail.com (G. Wang).

https://doi.org/10.1016/j.snb.2023.135038
Received 1 September 2023; Received in revised form 30 October 2023; Accepted 20 November 2023
Available online 22 November 2023

matrix to confine the fluorescent molecules by the electrostatic host-guest interaction [25]. Accordingly, HDS is also an ideal candidate for constructing AuNCs@HDS composite through electrostatic host-guest interaction. However, applying HDS as a matrix to confine AuNCs by electrostatic interaction for biosensing has rarely been investigated.

Inspired by the above investigations, this study reported the first attempt at confining glutathione-stabilized AuNCs on the surface of Zn-containing HDS (AuNCs@HDS) through a straightforward electrostatic interaction. This would result in constructing a highly efficient and versatile fluorescence strategy for sensing several vital bio-enzymes (Scheme 1). Due to the confinement effect of HDS, the AuNCs@HDS demonstrated excellent fluorescence performances (high QY, long fluorescence lifetime, and good stability). The p-nitrophenol (pNP) was validated to effectively quench the AuNCs@HDS fluorescence through a distinct inner filter effect (IFE) process. As pNP is the general product of many bio-enzyme-catalyzed pNP-substrate hydrolysis, the AuNCs@HDS was successfully employed for the versatile detection of several human diseases closely related bio-enzymes (β-GAL, β-GLU, and ALP) by varying the pNP-substrate. Besides, the remarkable sensitivity, satisfactory specificity, and accuracy in a serum test for bio-enzymes assay exemplified the robust analytical performance of this AuNCs@HDS-based platform for biosensing. As far as we know, it is the first study on designing highly fluorescent AuNCs-based nanocomposites for versatile fluorescent sensing of bio-enzymes.

2. Experimental section

2.1. Materials and equipment

β-Glucosidase (β-GLU), β-galactosidase (β-GAL), urate oxidase (UAox), glutathione transferase (GST), acetylcholinesterase (AChE), pepsin (PPS), lysozyme (LYS), tyrosinase (TYR), glutamic acid (Glu) and collagen (COL) were bought from Sigma-Aldrich (Shanghai, China). Alkaline phosphatase (ALP), glucose (GLC), p-nitrophenyl-phosphate (pNPP), hydrogen tetrachloroaurate (III) tetrahydrate ($HAuCl_4{\cdot}4\ H_2O$), glucose oxidase (GOX), urease (URE) and exonuclease III (Exo III) were bought from Shanghai Sangon Biotech Co., Ltd. p-Nitrophenyl-β-D-galactopyranoside (pNPGA), adenosine (A), valine (Val), serine (Ser) and guanosine (G) were gotten from Aladdin Inc. (Shanghai, China). Human serum albumin (HSA) was obtained from Dalian Meilun Biotechnology Co., LTD. (Dalian, China). p-Nitrophenyl-β-D-glucopyranoside (pNPGL) were bought from Shanghai Yuanye Bio-Technology Co., Ltd. Urea, proline (Pro), glycine (Gly), threonine (Thr), isoleucine (Ile) and other reagents (analytically pure) were obtained from Sinopharm Chemical Reagent Co., Ltd (Shanghai, China).

Fluorescence (FL) measurements were conducted on a PerkinElmer FL 6500 fluorescence spectrophotometer. UV–vis absorption spectra were acquired with a PerkinElmer UV/VIS Lambda 365 spectrophotometer. Fourier transform infrared (FT-IR) analysis was achieved on a Frontier PerkinElmer FT-IR spectrometer. Transmission electron microscopy (TEM), high resolution electron transmission microscopy (HRTEM), scanning transmission electron microscopy (STEM) and corresponding elemental mapping images were taken by a JEM-2100F Transmission Electron Microscope operating at 200 keV. Scanning electron microscopy (SEM) were performed on a JCM 7000 (JEOL, Ltd.). Fluorescence decays were performed with a Fluorescence Lifetime and Steady State Spectroscopy (FLS920, Edinburgh Instrument). The absolute fluorescence quantum yields were obtained in a calibrated integrating sphere in FLS920 spectrometer. X-ray photoelectron spectroscopy (XPS) was performed on a Thermo Scientific ESCALAB 250Xi using monochromatic Al Kα radiation (1486.68 eV) for the analysis of the surface composition and chemical states of the product. Powder X-ray diffraction (PXRD) patterns were conducted on a Bruker D8 ADVANCE. Zeta potentials were obtained from a Litesizer 500 analyzer at 25 ℃.

2.2. Synthesis of AuNCs@HDS composite

For the preparation of AuNCs@HDS, 1.5 mg HDS was added into 25 mL H_2O and then treated by sonication for 1 h. Subsequently, AuNCs (5 mL, 1.5 mg/mL) were introduced into the above solution. The mixed solution was allowed to react for 12 h. Finally, the AuNCs@HDS was harvested by centrifugation (10,000 r/min, 10 min) and washed with H_2O for 3 times to remove excess AuNCs. The precipitate of AuNCs@HDS was freeze-dried to obtain the AuNCs@HDS powder.

2.3. Fluorescence detection of ALP, β-GLU, and β-GAL activity

In the typical process to quantitatively detect ALP activity, ALP (60 μL) with different activities and pNPP (140 μL, 2.5 mM) were injected into Tris-HCl buffer (pH 9.0, 100 μL, 10 mM), and the mixture was incubated at 37 °C for 60 min. Then, AuNCs@HDS (300 μL, 0.3 mg/mL) and Tris-HCl buffer (pH 9.0, 400 μL, 10 mM) were injected into the

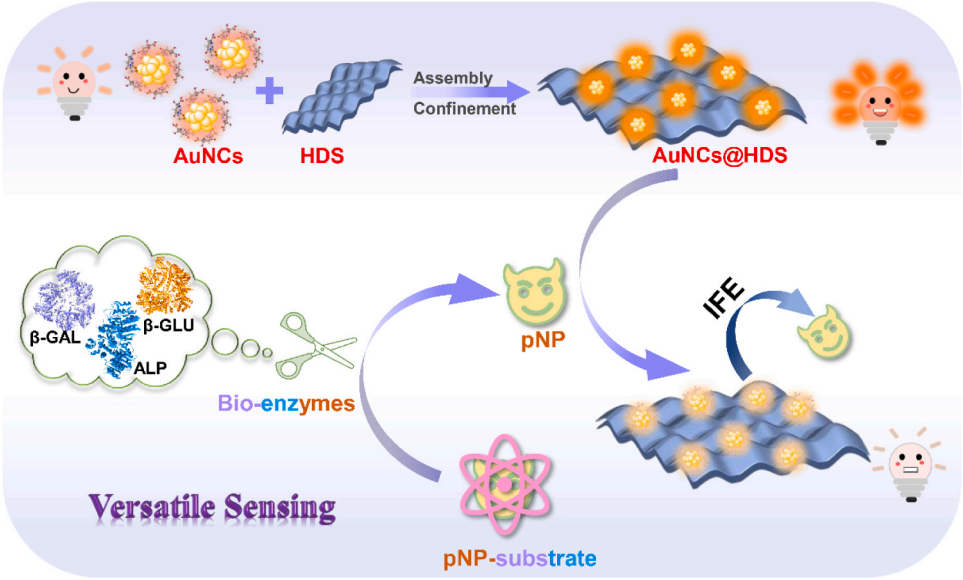

Scheme 1. Schematic diagram of a AuNCs@HDS-based versatile fluorescent sensing platform for detection of activity of bio-enzymes.

above mixtures. After fully mixed with 1 min, fluorescence emission spectra were performed under a single 405 nm excitation wavelength.

As for the detection of β-GLU, β-GLU (100 μL) with varied activities and pNPGL (120 μL, 2.5 mM) were injected into NaAc-HAc buffer (pH 5.0, 80 μL, 10 mM), and the mixture was reacted at 37 °C for 40 min. The following procedures were the same as those for ALP activity analysis.

The detection procedures of β-GAL activity were conducted as follows. pNPGA (100 μL, 2.5 mM), β-GAL (100 μL) with different concentrations and Tris-HCl buffer (pH 9.0, 100 μL, 10 mM) were mixed and incubated at 37 °C for 50 min. Then the experimental procedures were performed as the described procedures for ALP analysis.

2.4. Application to real samples

The prospective clinical prospect of the method to biological matrix was assessed by determining the bio-enzymes activity in the human serum samples. The human serum sample of healthy adults was collected from the Bethune First Hospital of Jilin University. The serum samples were processed by referring to the previous work [26]. In brief, the serum samples were first filtered by 0.45 μm filter membrane. Followed that, a centrifugation procedure at a speed of 12000 r/min for 20 min was conducted to remove the particulate matter of the serum samples. Finally, the standard addition methods were used to determine the detection performance of the proposed sensor for ALP, β-GLU, and β-GAL activity detection in serum samples, respectively.

3. Results and discussion

3.1. Materials synthesis and characteristics

The AuNCs were prepared through a one-pot synthesis method using a glutathione (GSH) as the reductant and template [27]. HDS was synthesized by reacting ZnO and aqueous $Zn(NO_3)_2$ aqueous solution at room temperature [25]. Next, the AuNCs@HDS was prepared by utilizing the electrostatic interactions between the positively charged HDS

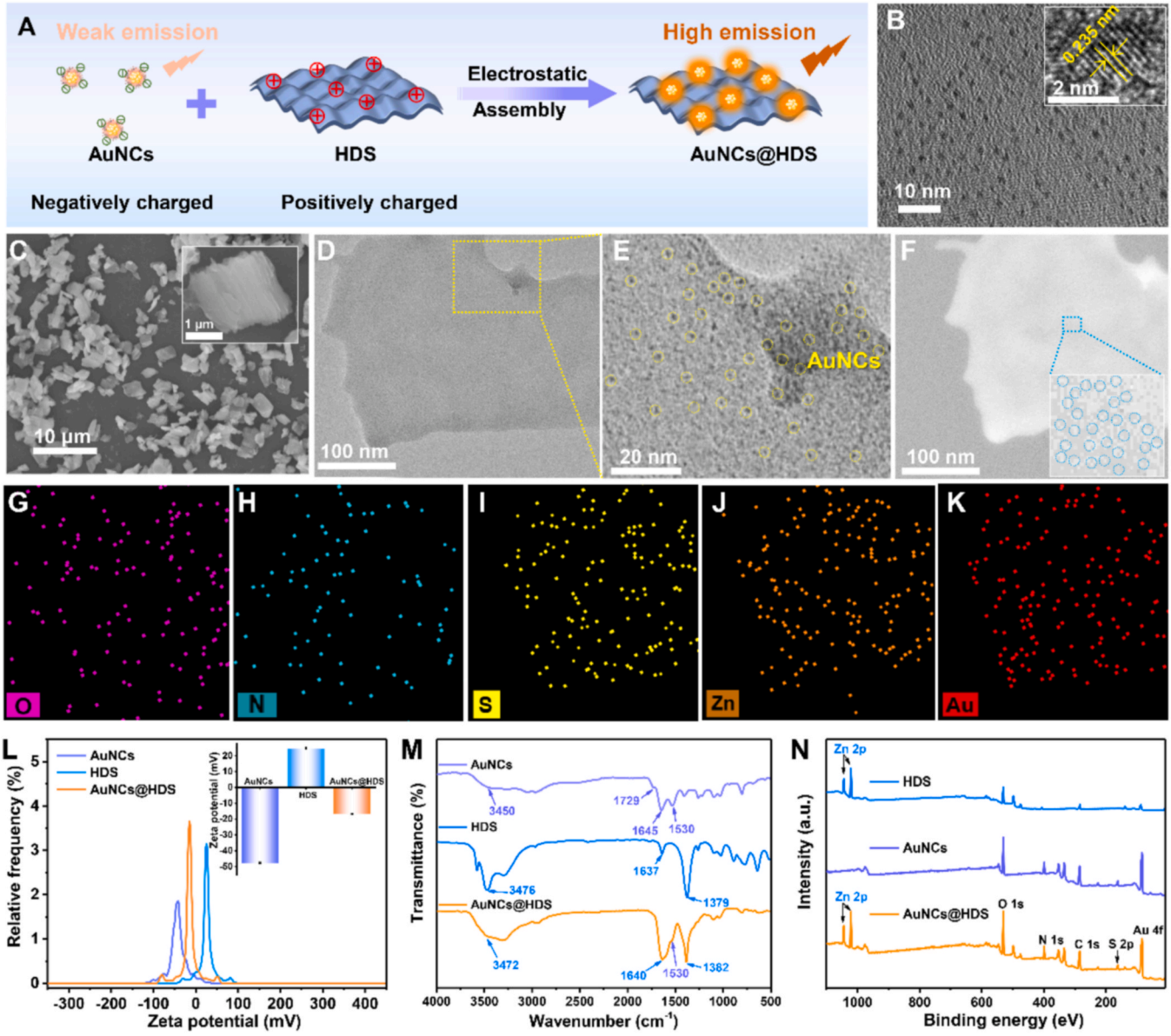

Fig. 1. (A) Illustration of AuNCs@HDS synthesis. (B–K) Morphology characterizations of AuNCs, HDS, and AuNCs@HDS. (B) TEM and HRTEM images of AuNCs. (C) SEM images of HDS. (D, E) TEM images of AuNCs@HDS. (F) STEM images and the N, S, Zn, and Au elemental mapping images (G–K) of AuNCs@HDS. Zeta potentials (L), FT-IR spectra (M), and XPS spectra (N) of AuNCs, HDS, and AuNCs@HDS, respectively.

and negatively charged AuNCs (Fig. 1A).

The morphologies of AuNCs, HDS, and AuNCs@HDS were thoroughly characterized by electron microscopy. The transmission electron microscopy (TEM) image in Fig. 1B revealed the prepared AuNCs monodispersed with a narrow size distribution and an average diameter of~ 2.05 nm (Fig. S1). The high-resolution TEM (HRTEM) image (Fig. 1B insert) demonstrated that the lattice planes were separated by 0.235 nm, attributed to the (111) lattice spacing of the face-centered cubic (fcc) Au [28]. The scanning electron microscopy (SEM) of HDS in Fig. 1C displayed that the HDS was a quadrilateral sheet of size < 5 μm.

SEM images of AuNCs@HDS revealed that the surface of HDS appeared to have a rough morphology after anchoring AuNCs (See Fig. S2). The AuNCs can be observed in the TEM image of AuNCs@HDS (Fig. 1D and E). As shown in Fig. 1E, the AuNCs (circled in yellow dash) were homogeneously anchored onto the HDS surface. Scanning transmission electron microscopy (STEM) demonstrated the distribution of AuNCs on HDS. Fig. 1F shows numerous AuNCs (white dots) evenly distributed throughout the HDS matrix. Additionally, Fig. 1G−K displays the energy-dispersive X-ray spectroscopy (EDS) elemental mapping of O, N, S, Au, and Zn from AuNCs and HDS, which indicates the homogeneous distribution of AuNCs on the HDS surface.

The zeta potential measurement further confirmed the formation of AuNCs@HDS, X-ray diffraction (XRD) patterns, Fourier transform infrared (FT-IR) spectra, and X-ray photoelectron spectra (XPS). The zeta potential analysis in Fig. 1L indicates that HDS was positively charged with an average zeta potential of + 24.6 mV, while the AuNCs were negatively charged with an average zeta potential of − 47.8 mV. Consequently, AuNCs can be adsorbed and confined onto the HDS surface due to the electrostatic interactions, forming the AuNCs@HDS composite. The AuNCs@HDS exhibited a partly neutralized zeta potential of − 16.7 mV after the self-assembly of AuNCs on the surface of HDS.

Fig. 1M shows the FT-IR spectra of AuNCs, HDS, and AuNCs@HDS. The AuNCs displayed a typical stretching N-H vibration at 1530 cm^{-1}. Besides, C═O stretching vibrations at 1729 cm^{-1}, O-H stretching at 3450 $cm^{-1,}$ and 1645 cm^{-1} were observed [29,30], indicating the existence of carboxyl groups on the AuNCs surface. For HDS, the stretching vibrations of N-O at 1379 cm^{-1} and that of O-H at 3476 cm^{-1} and 1637 cm^{-1} were clearly observed, confirming the existence of the hydroxyl groups and nitrate anions in HDS [25]. The FT-IR spectrum of AuNCs@HDS displays the distinct absorption peaks derived from AuNCs and HDS, demonstrating the successful self-assembly of AuNCs on the surface of HDS.

XPS and XRD were used to investigate the surface chemical composition and crystalline structures. Fig. 1N shows the XPS spectra of HDS, AuNCs, and AuNCs@HDS. The AuNCs and AuNCs@HDS had the same peaks at specific positions of 531, 400, 285, 163, 84 eV, which corresponded to O 1s, N 1s, C 1s, S 2p, and Au 4f, respectively [31,32]. Compared with the AuNCs, AuNCs@HDS displayed two typical binding energy peaks at 1020 eV and 1045 eV, attributed to the chemical states of low-energy band Zn $2p_{3/2}$ and high-energy band Zn $2p_{1/2}$ [33], indicating that AuNCs was successfully immobilized on HDS surface. Fig. S3 shows the XRD patterns of HDS, AuNCs, and AuNCs@HDS. The highly crystalline phase of HDS was confirmed by diffraction peaks corresponding to (003), (006), and (009) [25]. The layer spacing was calculated as 9.7 Å based on (003) reflections [34], suggesting that the AuNCs were only anchored on the surface of HDS due to the small layer spacing (9,7 Å) and was not sufficient to accommodate AuNCs with a diameter of 2.05 nm. The XRD pattern of AuNCs displays a typical diffraction peak at 33°, corresponding to the (111) plane of Au fcc structure [35], consistent with the lattice fringe results in Fig. 1B. The XRD pattern of AuNCs@HDS displays characteristic diffraction peaks of HDS and AuNCs, suggesting the successful formation of AuNCs@HDS composite.

3.2. Exploring the fluorescence properties and enhancement mechanism of AuNCs@HDS

The fluorescence properties and enhancement mechanism of AuNCs@HDS were systematically explored (Fig. 2A). Fig. 2B shows that the fluorescence emission of AuNCs was enhanced after being confined to the HDS surface, and the fluorescence emission peak exhibited a blue-shift from 603 to 587 nm. The CIE chromaticity diagrams of AuNCs (0.5328, 0.4577) and AuNCs@HDS (0.4936, 0.4841) further confirmed the fluorescence color change after the HDS confinement (See Fig. 2C). Fig. 2D revealed that the fluorescence enhancement effect was related to the weight ratio of HDS to AuNCs (w/w). As depicted in Fig. 2E, the fluorescence intensity of AuNCs@HDS gradually increased with increasing weight ratio, reaching a maximum value at HDS: AuNCs = 0.2:1 (w/w). This value was~ 8.5 times higher the original AuNCs. Correspondingly, the absolute fluorescence quantum yield (QY) of AuNCs@HDS was markedly improved to 22.80 %, 18.3 times that of the AuNCs (QY = 1.24 %). Besides, the fluorescence excitation spectra of AuNCs@HDS in Fig. S4 indicated that the maximum fluorescence excitation wavelength of AuNCs@HDS was located at 405 nm. From the summarized fluorescence lifetime data in Fig. 2F and Table S1, the average fluorescence lifetime of AuNCs and AuNCs@HDS were determined to be 2.53 μs and 11.19 μs. These results indicate the HDS confinement dramatically improved the fluorescence performance of AuNCs. The stability of AuNCs@HDS was also investigated. The AuNCs@HDS preserves 98 % of the initial intensity after 60 min of the Xe lamp irradiation (See Fig. S5A). Fig. S5B reveals that the AuNCs@HDS retained 90 % of the original value after 4 months of storage. Consequently, the confinement of HDS endowes excellent fluorescence properties and stability to AuNCs, improving the application prospects of AuNCs@HDS in biosensing.

First of all, due to that the absorption band edge of HDS of around 380 nm (Fig. S6) is lower than the fluorescence excitation wavelength of 405 nm (Fig. S4), excitation wavelength of 405 nm can not excite the HDS to generate photo-induced electrons and holes. Accordingly, the fluorescence enhancement originated from the transmission of photon-generated carrier from the HDS to AuNCs is excluded. The mechanism of the surface confinement effect was next explored. According to the principle of fluorescence property, when the excited electrons and holes are effectively confined by the matrix with a broad band gap to boost the recombination of electrons and holes, promoted radiation transition and enhanced fluorescence performances are observed [36–38]. Based on the above principle, the band edge placement investigation was conducted to reveal the confinement effect of the HDS on AuNCs (Fig. 2G and H). Fig. 2G shows the band gap values of HDS and AuNCs were calculated to be 3.25 and 2.29 eV. The valence band (VB) and conduction band (CB) of HDS were determined to be − 7.12 and − 3.87 eV (vs. vacuum); the calculated highest occupied molecular orbital (HOMO) and lowest unoccupied molecular orbital (LUMO) energies of AuNCs were − 6.52 and − 4.23 eV (vs. vacuum) (See the detailed calculation process in supporting information). Consequently, the excited electrons and hole cannot transfer to the conduction and valence bands of HDS (See Fig. 2I), respectively, facilitating the recombination of electrons/holes with improved fluorescence performances of AuNCs [19,39].

3.3. Constructing a versatile fluorescence sensing strategy

The outstanding fluorescence properties of AuNCs@HDS encouraged its biosensing applications. As a proof-of-concept, herein, a versatile AuNCs@HDS-based fluorescence strategy was constructed for sensing vital bio-enzymes by designing pNP as the "bridge" substance, including β-galactosidase (β-GAL), alkaline phosphatase (ALP) and β-glucosidase (β-GLU) (Scheme 1). The pNP efficiently quenched the fluorescence emission of AuNCs@HDS via the inner filter effect (IFE). As pNP is the general product of many bio-enzymes-catalyzed hydrolysis reactions, the AuNCs@HDS/pNP-based assay could be presumptively extended to

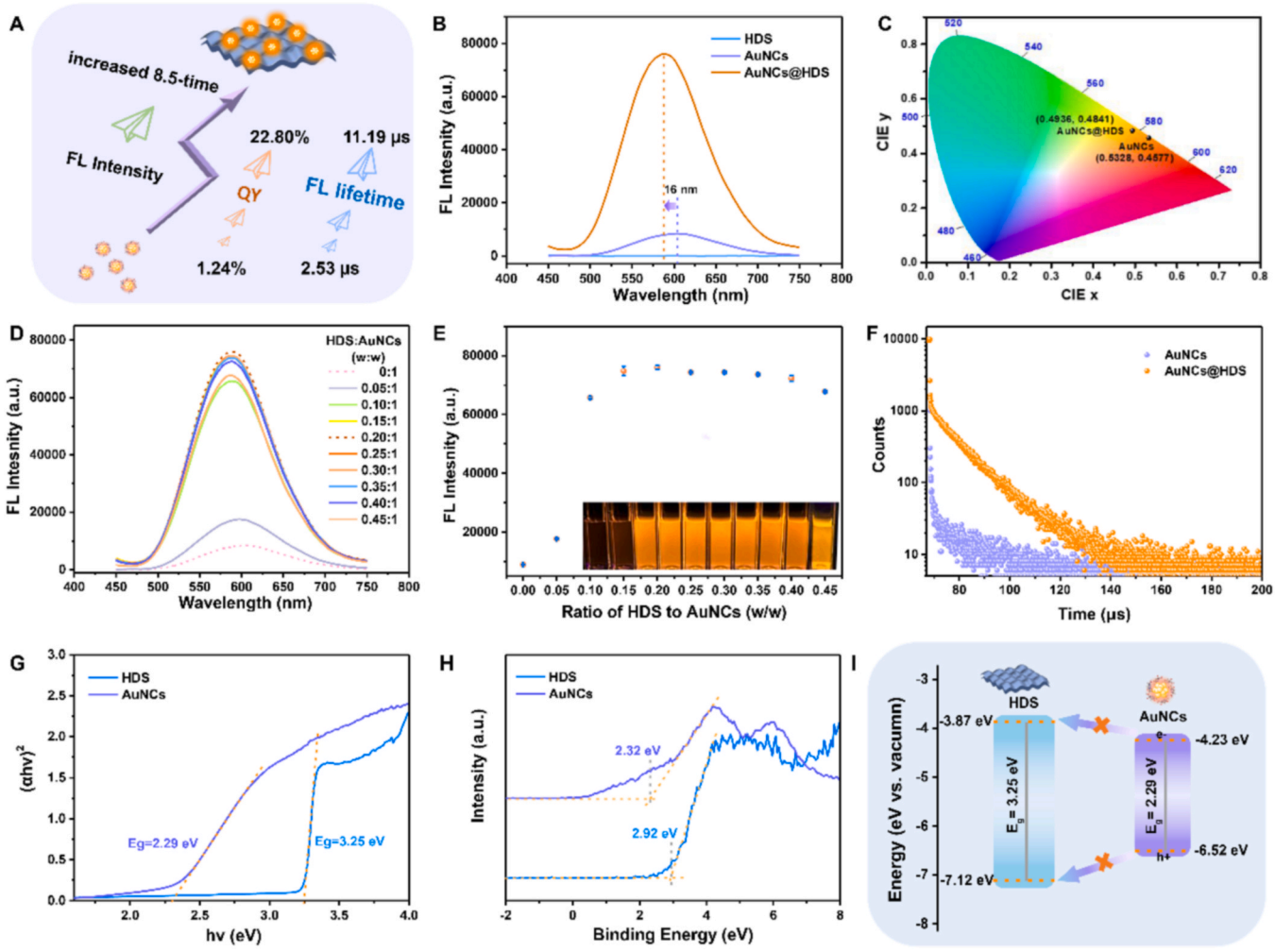

Fig. 2. . (A) Fluorescence properties of AuNCs and AuNCs@HDS. (B) Fluorescence emission spectra of AuNCs, HDS, and AuNCs@HDS, respectively. (C) CIE chromaticity diagram of AuNCs and HDS@AuNCs. Fluorescence emission spectra (D) and intensity (E) of AuNCs@HDS at different ratios (by weight) of HDS to AuNCs. Inset: the corresponding digital photo of AuNCs@HDS under UV irradiation. (F) Fluorescence decay curves of AuNCs and HDS@AuNCs. (G) Band gap energies of HDS and AuNCs. (H) XPS valence band spectra of HDS and AuNCs. (I) Band edge placement of AuNCs, HDS, and AuNCs@HDS.

a versatile assay of β-GAL, β-GLU, and ALP by varying the pNP-substrate/bio-enzyme pair. The following measurements further verified the mechanism and validity of our platform for these bio-enzyme sensing.

First, the underlying mechanism of pNP-regulated fluorescence quenching of AuNCs@HDS was investigated. Typically, static quenching, dynamic quenching, and inner filter effect (IFE) are the most common quenching mechanisms responsible for the fluorescence quenching phenomenon [40,41]. Among the varied mechanisms, static quenching occurs when a ground-state complex is formed through the intense interaction between the fluorophore and quencher [42,43]. Fig. 3A shows that pNP and AuNCs@HDS were all negatively charged with zeta potentials of − 51.0 mV and − 16.7 mV, respectively, indicating electrostatic repulsion between pNP and AuNCs@HDS. This electrostatic repulsive force inhibited the complex formation between pNP and AuNCs@HDS. Fig. 3B shows that the absorption spectrum of the AuNCs@HDS/pNP system was similar to that from the direct theoretical sum of the absorption spectra of the pNP@AuNCs and HDS, implying there was no interaction or ground-state complex formation between pNP and AuNCs@HDS [44]. Accordingly, the possibility of static quenching could be excluded from the pNP/AuNCs@HDS sensing system.

In a dynamic quenching system, the fluorescence lifetime of the fluorophores can be changed by the quenchers since the energy or electron transfer happens in the excited state, substantially affecting the fluorescence lifetime of the fluorophores [45,46]. Therefore, the fluorescence lifetimes of the AuNCs@HDS with and without pNP were measured. Fig. 3C and Table S1 show that the fluorescence lifetime of AuNCs@HDS exhibited little change with the introduction of pNP, implying that no energy transfer or electron transfer occurred in the pNP/AuNCs@HDS sensing system. Thus, the possibility of dynamic quenching could also be excluded.

Inner filter effect (IFE) is a kind of efficient fluorescence quenching behavior originating from the absorption of excitation and/or emission light of fluorophores by the quenchers [47,48]. IFE has some distinguishable characteristics of IFE compared with static and dynamic quenching. (a) No direct interactions between fluorophores and quenchers occur in the IFE. Subsequently, the absorption peaks of the fluorophore show no changes, and no new substance is formed. (b) No fluorescence lifetime changes are observed during the IFE because no excited-state energy or electron transfer is involved in the quenching process. (c) A prerequisite for IFE is the overlap of the absorption spectra of the quenchers with the fluorescence emission and/or excitation spectra of fluorophores. Fig. 3D shows a precise overlap between the FL excitation spectra of AuNCs@HDS and the absorption spectrum of pNP, implying that pNP can effectively absorb the excitation light of AuNCs@HDS. The above results showed no interaction between pNP and AuNCs@HDS (Fig. 3A and B), a negligible change of lifetime

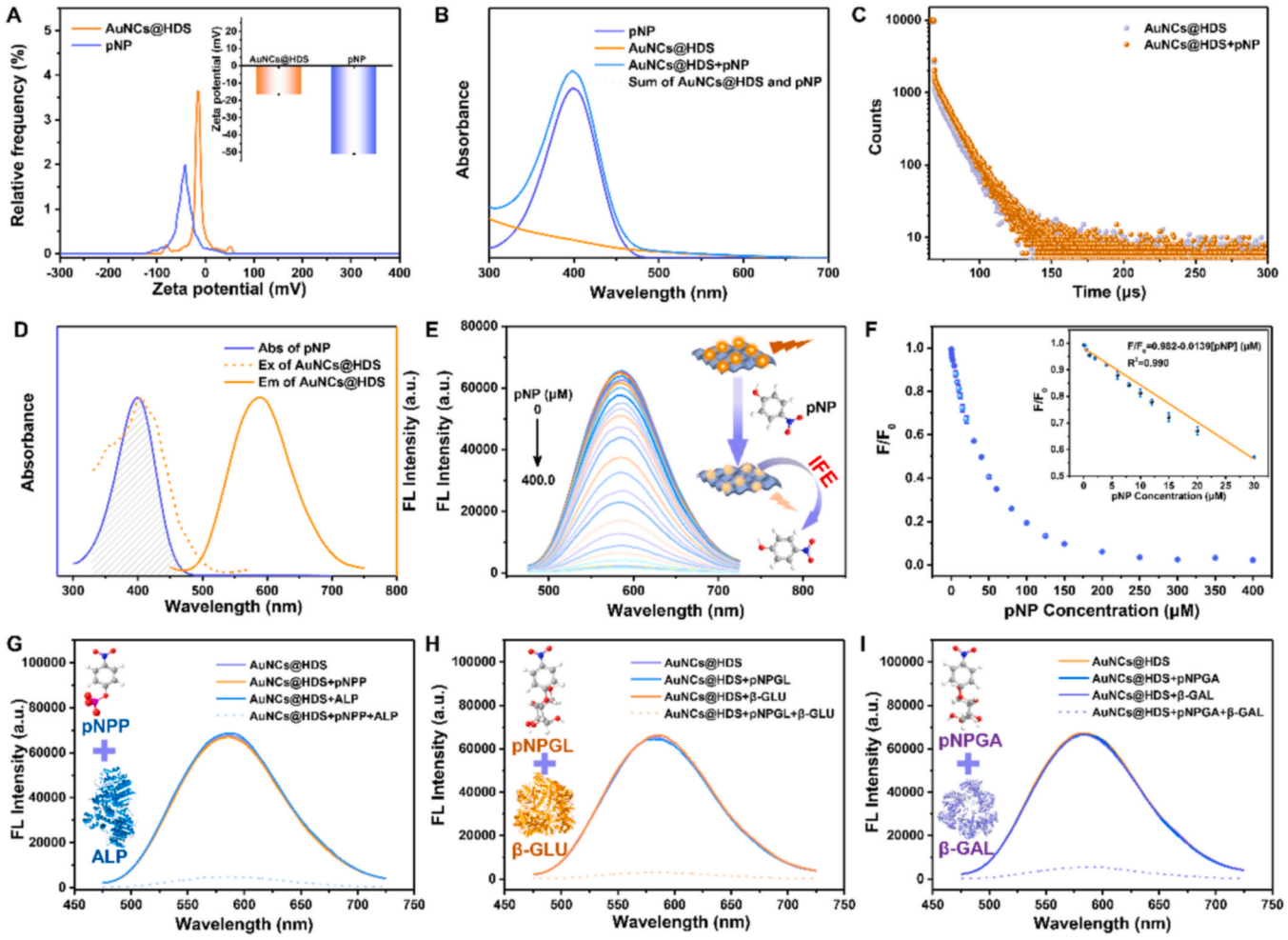

Fig. 3. . (A) Zeta potentials of AuNCs@HDS and pNP. (B) UV–vis absorption spectra of pNP, AuNCs@HDS, pNP/AuNCs@HDS, and a sum of pNP and AuNCs@HDS. (C) Fluorescence decay curves of AuNCs@HDS and pNP/AuNCs@HDS system. (D) UV–vis absorption spectra of pNP. Fluorescence excitation and emission spectra of AuNCs@HDS. (E) Fluorescence emission spectra of AuNCs@HDS in the presence of varied amounts of pNP. (F) A plot of the fluorescence intensity ratio (F/F_0) and pNP amount. (G-I) Fluorescence emission spectra of the AuNCs@HDS system with blank, pNP-substrate (pNPP, pNPGL, pNPGA), bio-enzyme (ALP, β-GLU, and β-GAL), and pNP-substrate/bio-enzyme (pNPP/ALP, pNPGL/β-GLU and pNPGA/β-GAL).

(Fig. 3C), and sufficient spectral overlap (Fig. 3D). These are typical properties of IFE, indicating that the IFE during pNP and AuNCs@HDS caused fluorescence quenching.

Based on the above mechanism, a biosensing platform was employed to detect pNP. The recognition performance of pNP directly affected the sensitivity of related bio-enzymes sensing. Under the optimum pH of 9.0 and incubation time of 1 min (shown in Fig. S7A and Fig. S7B), the fluorescence of AuNCs@HDS was gradually quenched by the increasing concentration of pNP (0–400.0 μM) (See Fig. 3E). And the quenching efficiency exceeded 99.7% when the concentration of pNP was 400.0 μM. A good linearity was observed between the fluorescence intensity ratio F/F_0 (F and F_0 displayed the AuNCs@HDS/pNP system fluorescence intensity without and with pNP) and pNP concentration in the range of 0.1 − 30.0 μM (Fig. 3F). The regression equation was $F/F_0 = 0.982 - 0.0139[pNP]$ (μM) with $R^2 = 0.990$. The detection limit (LOD) for pNP was as low as 33.1 nM. The sensitive measurement of pNP enabled the construction of a sensing platform for bio-enzymes activity.

Bio-enzymes have the essential function of controlling various physiological processes in an organism [49]. Most bio-enzymes have been validated as biomarkers with applications in medical biochemistry, such as disease diagnosis and drug screening. Since pNP is the general product of many bio-enzymes-catalyzed hydrolysis reactions, the AuNCs@HDS/pNP-based assay can be presumptively extended to the assay of several critical bio-enzymes by varying the pNP-substrate/bio-enzyme pair (Fig. S8 and Fig. S9), including p-nitrophenyl-β-D-galactopyranoside (pNPGA)/β-GAL, p-nitrophenyl-β-D-glucopyranoside (pNPGL)/β-GLU and p-nitrophenyl-phosphate (pNPP)/ALP.

The feasibility of this versatile approach for bio-enzymes sensing was verified. Fig. S10 shows a typical absorption peak at 405 nm due to the generated pNP in the UV–vis spectra after the catalysis of the pNP substrate by its corresponding bio-enzyme. This result confirms pNP generation in different pNP-substrate/bio-enzyme (pNPP/ALP, pNPGL/β-GLU, and pNPGA/β-GAL) systems. Besides, the individual substrate (pNPGA, pNPGL, pNPP) or bio-enzymes (ALP, β-GLU, and β-GAL) displays no effect on the fluorescence spectra of AuNCs@HDS (See Fig. 3G−I). As expected, with the introduction of pNPGA/β-GAL, pNPGL/β-GLU or pNPP/ALP into the AuNCs@HDS system, there is a decrease in the fluorescence of AuNCs@HDS, verifying the feasibility of this system for versatile bio-enzymes sensing.

3.4. *Analytical performance of the ALP, β-GLU, and β-GAL activity assay*

The AuNCs@HDS-based quantitative detections of ALP, β-GLU, and β-GAL activity were performed by varying the pNP-substrate under optimal experimental conditions (Fig. S11−S13). Fig. 4A shows that the fluorescence emission of pNPP/AuNCs@HDS at 587 nm gradually decreases with increasing ALP activity from 0 to 20.0 U/L. Fig. 4B shows

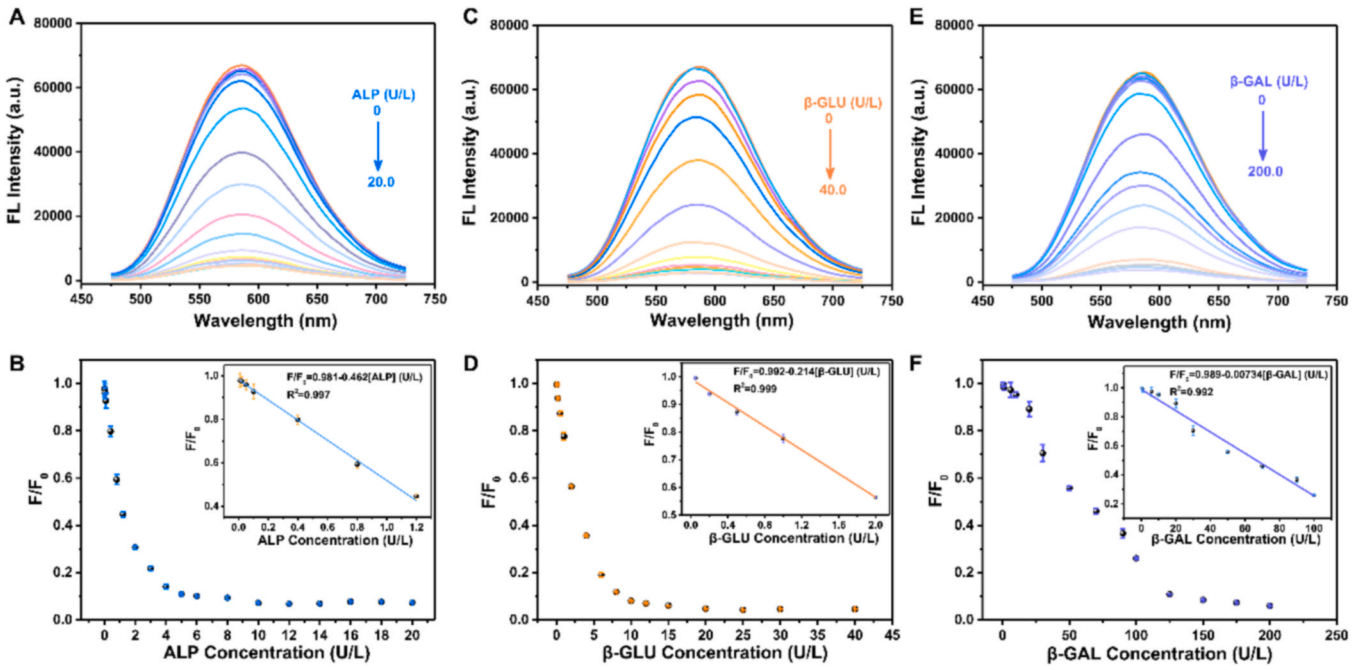

Fig. 4. Fluorescence emission spectra (A) and intensity (B) of pNPP/AuNCs@HDS with varied ALP concentrations. Fluorescence emission spectra (C) and intensity (D) of pNPGL/AuNCs@HDS in the presence of varied β-GLU. Fluorescence emission spectra (E) and intensity (F) of pNPGA/AuNCs@HDS with varied β-GAL concentrations.

the plots of fluorescence intensity ratio (F/F_0) exhibited an excellent linear relationship between 0.01 and 1.2 U/L (F/F_0 = 0.981–0.462 [ALP], U/L, R^2 = 0.997) with a LOD value of 0.0092 U/L. The LOD of this assay is much lower than that of most reported methods (See Table S2), indicating that the platform could efficiently detect ALP.

Fig. 4C shows that the fluorescence intensity of pNPGL/AuNCs@HDS gradually increased with increasing β-GLU concentration in the 0–40.0 U/L range. The fluorescence intensity ratio (F/F_0) is proportional to the concentration of β-GLU from 0.05 U/L to 2.0 U/L, and a calibration equation of F/F_0 = 0.992–0.214[β-GLU], U/L (R^2 = 0.999) is obtained (See Fig. 4D). The LOD is 0.029 U/L. The results are comparable to previously reported methods for β-GLU measurement (Table S3), confirming that this platform provided gratifying sensitivity for β-GLU.

With pNPGA as substrate, a gradual decrease of fluorescence of the pNPGA/AuNCs@HDS system is observed in Fig. 4E when the concentration of β-GAL increases from 0 to 200.0 U/L. Further, the fluorescence intensity ratio plots showed a linear relationship (F/F_0 = 0.989–0.00734 [β-GAL], R^2 = 0.992) in the range of 0.5–100.0 U/L (Fig. 4F). The LOD of β-GAL is calculated as 0.27 U/L. The high sensitivity of this method for β-GAL sensing is revealed by comparing this assay with reported methods for detecting GLU (See Table S4).

3.5. *Specificity and practical applications of the AuNCs@HDS-based platform*

The specificity of this AuNCs@HDS-based platform was measured by investigating its responses to the common electrolytes and biological species (depicted in different colors in Fig. 5), including common ions (purple), bio-enzymes (orange), amino acids (blue), and other biomolecules (green). In ALP detection, other species display no evident impacts on the fluorescence intensity of the AuNCs@HDS/pNPP system compared with the blank (See Fig. 5A). The anti-interference ability of the sensing system was assessed by the addition of these substances into the AuNCs@HDS/pNPP/ALP system (See Fig. 5B). As revealed in Fig. 5B, the pNPP/ALP/AuNCs@HDS system exhibits the identical responses to ALP in the presence of these foreign substances, demonstrating the satisfactory anti-interference capability of the sensor for ALP activity determination. As revealed in Fig. 5C-F, the AuNCs@HDS-based platform also exhibits good specificity for β-GLU and β-GAL sensing similar to ALP.

Human serum samples were picked as the representative biological model to demonstrate the practical biosensing applications of the AuNCs@HDS-based platform. A standard addition method was applied to test ALP, β-GLU, and β-GAL activity separately in healthy human serum samples. Fig. S14 demonstrates that the human serum samples 1–3 (200-fold diluted) did not cause any interference in the biosensing by the AuNCs@HDS. The classic colorimetric assays for these bio-enzymes were adopted as the reference methods to evaluate the accuracy of this method (Fig. S15–S17). As revealed in Table S5, the recovery of this method for ALP detection varies from 90.00 % to 106.67 %, with relative standard deviations (RSDs) < 3.4 %. As for β-GLU and β-GAL, the recovery of this method for β-GLU varies from 94.00 % to 104.00 % with RSDs < 3.3 % (Table S6). The recoveries of β-GAL ranges from 90.13 % to 101.80 %, and RSDs were no more than 4.9 % (Table S7). Besides, the analysis results of this proposed method are consistent with those of the reference colorimetric method (Table S5–S7). The results demonstrate this versatile approach's excellent accuracy and reliability for sensing bio-enzymes (ALP, β-GLU, and β-GAL) activity. These results suggested that the AuNCs@HDS material provides promising technical tools for practical clinical diagnosis related to biological enzymes. Meanwhile, the exhibited robust performance of AuNCs@HDS indicated its great application possibility for other biosensing applications, such as environmental monitoring, and food analysis.

4. Conclusion

In this study, immobilized AuNCs@HDS with high QY and stability were conducted by an electrostatic confinement strategy and were rationally designed for highly efficient and versatile sensing of various vital bio-enzymes for the first time. This work exhibited the following features. (1) The AuNCs@HDS were prepared by electrostatic interaction between the negatively charged AuNCs and positively charged HDS. The preparation did not involve tedious experimental procedures, costly reagents, or toxic chemicals. (2) Due to the strong confinement effect of

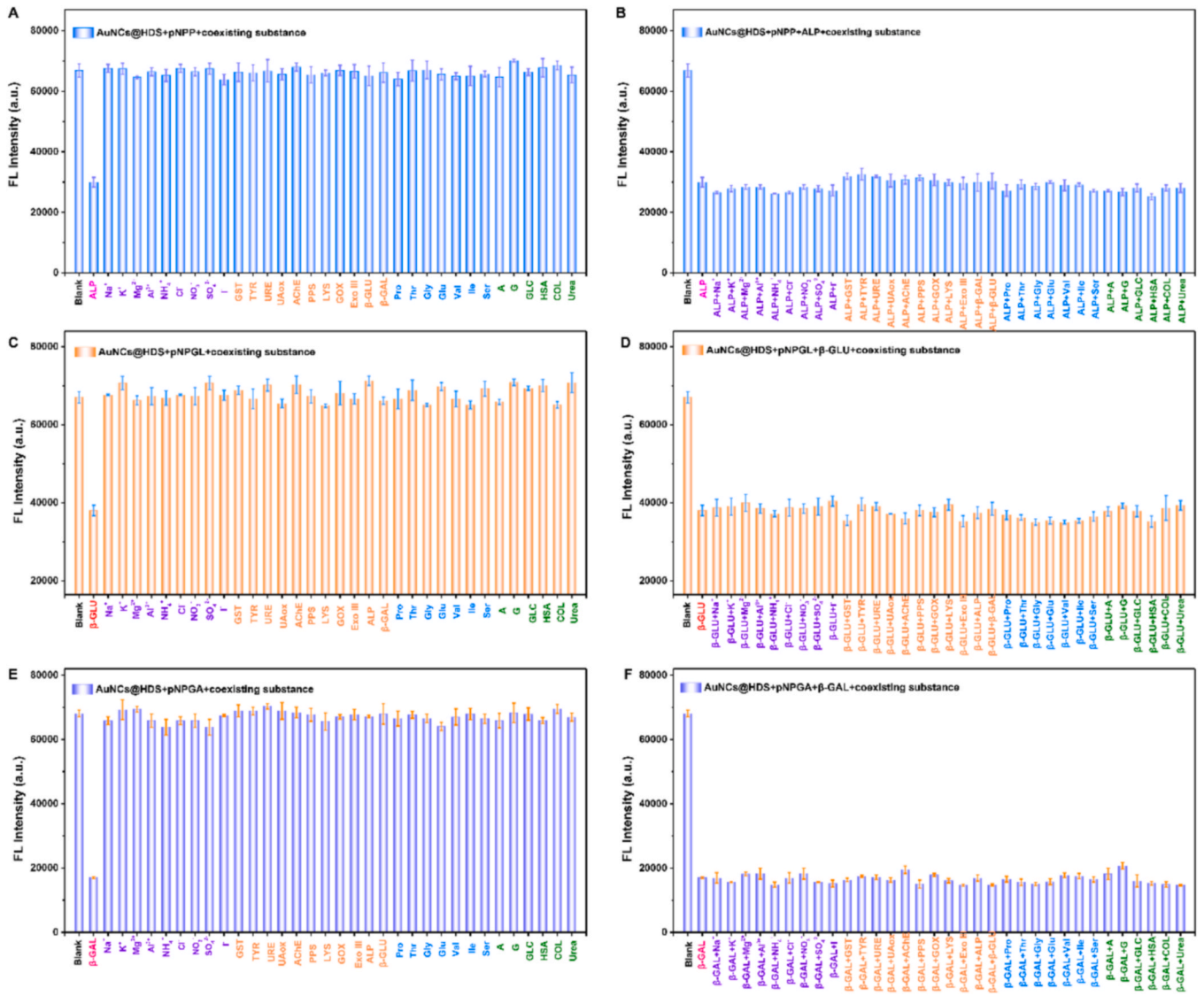

Fig. 5. Selectivity of the AuNCs@HDS-based method for ALP (A), β-GLU (C), and β-GAL (E) detection. Anti-interference ability of the system for ALP (B), β-GLU (D), and β-GAL (F) with the addition of interfering substances. Concentrations: 1.2 U/L ALP, 2.0 U/L β-GLU, 100.0 U/L β-GAL, and other bio-enzymes, 10.0 μg/mL COL and HSA, 50.0 μM ions, amino acids, and other bio-molecules.

HDS, the fabricated AuNCs@HDS displayed 8.5 times enhanced fluorescence intensity, much higher QY (22.80 % vs. 1.24 %), and prolonged fluorescence lifetime (11.19 μs vs. 2.53 μs) compared with AuNCs. (3) A convenient, highly sensitive, and specific AuNCs@HDS-based versatile strategy was successfully constructed to detect ALP, β-GLU, and β-GAL with robust analysis capabilities. This work is expected to offer a simple yet effective avenue to use the HDS-based confinement effect for fabricating the AuNCs/HDS probe with high fluorescence performance. This study will also contribute to biosensing applications by applying AuNCs/HDS as promising substitutes for the probes.

CRediT authorship contribution statement

Mengke Wang: Conceptualization, Investigation, Validation, Funding acquisition , Formal analysis, Writing - Original Draft. **Yaqing Han**: Investigation, Data Curation, Formal analysis, Software. **Rui Huang**: Resources. **Zhonghao Wang**: Software. **Guannan Wang**: Supervision, Funding acquisition, Project administration, Writing - Review & Editing.

Declaration of Competing Interest

The authors declare that they have no known competing financial interests or personal relationships that could have appeared to influence the work reported in this paper.

Data availability

Data will be made available on request.

Acknowledgments

This work is supported by Natural Science Foundation of Shandong Province (ZR2023QB126), Higher Education Institutions' Youth Innovation Team of Shandong Province (600768002), and the Doctoral Scientific Research Foundation of Jining Medical University (601018001).

Appendix A. Supporting information

Supplementary data associated with this article can be found in the

online version at doi:10.1016/j.snb.2023.135038.

References

[1] Y.G. Srinivasulu, Q. Yao, N. Goswami, J. Xie, Interfacial engineering of gold nanoclusters for biomedical applications, Mater. Horiz. 7 (2020) 2596–2618.
[2] K. Kwak, D. Lee, Electrochemistry of atomically precise metal nanoclusters, Acc. Chem. Res. 52 (2019) 12–22.
[3] C.N. Loynachan, A.P. Soleimany, J.S. Dudani, Y. Lin, A. Najer, A. Bekdemir, et al., Renal clearable catalytic gold nanoclusters for in vivo disease monitoring, Nat. Nanotechnol. 14 (2019) 883–890.
[4] D.L. Li, Q. Liu, Q.R. Qi, H. Shi, E.C. Hsu, W.Y. Chen, et al., Gold nanoclusters for NIR-II fluorescence imaging of bones, Small 16 (2020), 2070237.
[5] Y.Z.Y. Xie, Y.L. Xianyu, N.X. Wang, Z.Y. Yan, Y. Liu, K. Zhu, et al., Functionalized gold nanoclusters identify highly reactive oxygen species in living organisms, Adv. Funct. Mater. 28 (2018), 1702026.
[6] M. Cui, Y. Zhao, Q. Song, Synthesis, optical properties and applications of ultra-small luminescent gold nanoclusters, Trends Anal. Chem. 57 (2014) 73–82.
[7] I. Mahmood Khan, S. Niazi, W. Akhtar, L. Yue, I. Pasha, M.K.I. Khan, et al., Surface functionalized AuNCs optical biosensor as an emerging food safety indicator: fundamental mechanism to future prospects, Coord. Chem. Rev. 474 (2023), 214842.
[8] H. Wang, Q. Li, J. Zhang, H. Zhang, Y. Shu, Z. Zhao, et al., Visualization and manipulation of solid-state molecular motions in cocrystallization processes, J. Am. Chem. Soc. 143 (2021) 9468–9477.
[9] X. Hu, Y. Zheng, J. Zhou, D. Fang, H. Jiang, X. Wang, Silver-assisted thiolate ligand exchange induced photoluminescent boost of gold nanoclusters for selective imaging of intracellular glutathione, Chem. Mater. 30 (2018) 1947–1955.
[10] X. Ran, Z. Wang, F. Pu, E. Ju, J. Ren, X. Qu, Nucleic acid-driven aggregation-induced emission of Au nanoclusters for visualizing telomerase activity in living cells and in vivo, Mater. Horiz. 8 (2021) 1769–1775.
[11] Y. Cai, Z. Qiu, X. Lin, W. Zeng, Y. Cao, W. Liu, et al., Self-assembled nanomaterials based on aggregation-induced emission of AuNCs: Fluorescence and colorimetric dual-mode biosensing of organophosphorus pesticides, Sens. Actuators B: Chem. 321 (2020), 128481.
[12] S.X. Wang, X.M. Meng, A. Das, T. Li, Y.B. Song, T.T. Cao, et al., A 200-fold quantum yield boost in the photoluminescence of silver doped AgxAu25-x nanoclusters: the 13 th silver atom matters**, Angew. Chem. -Int. Ed. 53 (2014) 2376–2380.
[13] M. Wang, X. Zhou, X. Wang, M. Wang, X. Su, One-step fabrication of wavelength-tunable luminescence of gold-silver bimetallic nanoclusters: robust performance for α-glucosidase assay, Sens. Actuators B: Chem. 345 (2021), 130407.
[14] R. Tian, S. Zhang, M. Li, Y. Zhou, B. Lu, D. Yan, et al., Localization of Au nanoclusters on layered double hydroxides nanosheets: confinement-induced emission enhancement and temperature-responsive luminescence, Adv. Funct. Mater. 25 (2015) 5006–5015.
[15] R. Jalili, M. Dastborhan, S. Chenaghlou, A. Khataee, Incorporating of gold nanoclusters into metal-organic frameworks for highly sensitive detection of 3-nitrotyrosine as an oxidative stress biomarker, J. Photochem. Photobiol. A: Chem. 391 (2020), 112370.
[16] X. Bai, S. Xu, L. Wang, Full-range pH ctable Au-clusters in nanogel for confinement-enhanced emission and improved sulfide sensing in living cells, Anal. Chem. 90 (2018) 3270–3275.
[17] D. Wei, M. Li, Y. Wang, N. Zhu, X. Hu, B. Zhao, et al., Encapsulating gold nanoclusters into metal-organic frameworks to boost luminescence for sensitive detection of copper ions and organophosphorus pesticides, J. Hazard. Mater. 441 (2023), 129890.
[18] L.K. Sarpong, M. Bredol, M. Schonhoff, A. Wegrzynowicz, K. Jenewein, H. Uphoff, One-pot synthesis of carbon nanotube/zinc sulfide heterostructures: characterization and effect of electrostatic interaction on the optical properties, Opt. Mater. 86 (2018) 398–407.
[19] J.L. Yang, N.Z. Song, Q. Jia, Investigation of the surface confinement effect of copper nanoclusters: construction of an ultrasensitive fluorescence turn-on bio-enzyme sensing platform, Nanoscale 11 (2019) 21927–21933.
[20] S. Li, H. Zhang, Z. Huang, Q. Jia, Spatially confining copper nanoclusters in porous ZrO_2 for fluorescence/colorimetry/smartphone triple-mode detection of metoprolol tartrate, Biosens. Bioelectron. 231 (2023), 115290.
[21] S.H. Chen, Z. Li, W.J. Li, Z.Z. Huang, Q. Jia, Confining copper nanoclusters on exfoliation-free 2D boehmite nanosheets: fabrication of ultra-sensitive sensing platform for alpha-glucosidase activity monitoring and natural anti-diabetes drug screening, Biosens. Bioelectron. 182 (2021), 113198.
[22] S.H. Chen, Z. Li, R.S. Xue, Z.Z. Huang, Q. Jia, Confining copper nanoclusters in three dimensional mesoporous silica particles: fabrication of an enhanced emission platform for "turn off-on" detection of acid phosphatase activity, Anal. Chim. Acta 1192 (2022), 339387.
[23] G.R. Williams, J. Crowder, J.C. Burley, A.M. Fogg, The selective intercalation of organic carboxylates and sulfonates into hydroxy double salts, J. Mater. Chem. 22 (2012) 13600–13611.
[24] A.Y.A. Kaassis, S.M. Xu, S.Y. Guan, D.G. Evans, M. Wei, G.R. Williams, Hydroxy double salts loaded with bioactive ions: synthesis, intercalation mechanisms, and functional performance, J. Solid State Chem. 238 (2016) 129–138.
[25] J.L. Yang, Z. Li, Q. Jia, Anchoring copper nanoclusters to Zn-containing hydroxy double salt: construction of 2D surface confinement induced enhanced emission toward bio-enzyme sensing and light-emitting diode fabrication, Chem. Commun. 56 (2020) 3081–3084.
[26] Q.F. Zhai, H.H. Xing, D.Q. Fan, X.W. Zhang, J. Li, E.K. Wang, Gold-silver bimetallic nanoclusters with enhanced fluorescence for highly selective and sensitive detection of glutathione, Sens. Actuators B-Chem. 273 (2018) 1827–1832.
[27] Z. Luo, X. Yuan, Y. Yu, Q. Zhang, D.T. Leong, J.Y. Lee, et al., From aggregation-induced emission of Au(I)-thiolate complexes to ultrabright Au(0)@Au(I)-thiolate core-shell nanoclusters, J. Am. Chem. Soc. 134 (2012) 16662–16670.
[28] Y.-G. Feng, J.-H. Zhu, A.-J. Wang, L.-P. Mei, X. Luo, J.-J. Feng, AuPt nanocrystals/polydopamine supported on open-pored hollow carbon nanospheres for a dual-signaling electrochemical ratiometric immunosensor towards h-FABP detection, Sens. Actuators B: Chem. 346 (2021), 130501.
[29] N.A. Devi, S. Sinha, S. Nongthombam, B.P. Swain, Structural, optical, electrochemical and electrical studies of Bi2O3@rGO nanocomposite, Mater. Sci. Semicond. Process. 137 (2022), 106212.
[30] H.D. Ruan, R.L. Frost, J.T. Kloprogge, The behavior of hydroxyl units of synthetic goethite and its dehydroxylated product hematite, Spectrochim. Acta Part A: Mol. Biomol. Spectrosc. 57 (2001) 2575–2586.
[31] N. Blondiaux, S. Zuercher, M. Liley, N.D. Spencer, Fabrication of multiscale surface-chemical gradients by means of photocatalytic lithography, Langmuir 23 (2007) 3489–3494.
[32] R. del Caño, J.M. Gisbert-González, J. González-Rodríguez, G. Sánchez-Obrero, R. Madueño, M. Blázquez, et al., Effective replacement of cetyltrimethylammonium bromide (CTAB) by mercaptoalkanoic acids on gold nanorod (AuNR) surfaces in aqueous solutions, Nanoscale 12 (2020) 658–668.
[33] N. Gogurla, A.K. Sinha, S. Santra, S. Manna, S.K. Ray, Multifunctional Au-ZnO plasmonic nanostructures for enhanced UV photodetector and room temperature NO sensing devices, Sci. Rep. 4 (2014), 6483.
[34] J.Y. Lu, C.X. Xu, Z.S. Tian, J.F. Lu, Y. Lin, Z.L. Shi, Green emission and Ag^+ sensing of hydroxy double salt supported gold nanoclusters, Nanoscale 8 (2016) 5120–5125.
[35] M. Jafari, J. Tashkhourian, G. Absalan, Chiral recognition of naproxen enantiomers based on fluorescence quenching of bovine serum albumin-stabilized gold nanoclusters, Spectrochim. Acta Part a-Mol. Biomol. Spectrosc. 185 (2017) 77–84.
[36] S.-S. Chen, H. Wang, B. Wu, Q. Li, J. Gong, Y.-L. Zhao, et al., Natural coumarin isomers with dramatically different AIE properties: mechanism and application, ACS Cent. Sci. 9 (2023) 883–891.
[37] L. Fu, H. Liu, L. Yan, Y. Fu, Y. Zhu, L. Jin, et al., Fabrication of CuNCs/LDHs films with excellent luminescent properties and exploration of thermosensitivity, Ind. Eng. Chem. Res. 58 (2019) 8009–8015.
[38] J. Yang, Y. Peng, S. Li, J. Mu, Z. Huang, J. Ma, et al., Metal nanocluster-based hybrid nanomaterials: fabrication and application, Coord. Chem. Rev. 456 (2022), 214391.
[39] R. Tian, D. Yan, C. Li, S. Xu, R. Liang, L. Guo, et al., Surface-confined fluorescence enhancement of Au nanoclusters anchoring to a two-dimensional ultrathin nanosheet toward bioimaging, Nanoscale 8 (2016) 9815–9821.
[40] J. Sun, J.H. Zhao, L. Wang, H.W. Li, F. Yang, X.R. Yang, Inner filter effect-based sensor for horseradish peroxidase and its application to fluorescence immunoassay, ACS Sens. 3 (2018) 183–190.
[41] M.P. Ajith, S. Pardhiya, P. Rajamani, Carbon dots: an excellent fluorescent probe for contaminant sensing and remediation, Small 18 (2022), 2105579.
[42] F. Chen, B.X. Zhang, Z.J. Ding, M. Zhong, Y.A. Hou, F. Zhang, et al., Hemin as a general static dark quencher for constructing heme oxygenase-1 fluorescent probes, Angew. Chem. -Int. Ed. (2023), e202301598.
[43] T. Skorjanc, D. Shetty, M. Valant, Covalent organic polymers and frameworks for fluorescence-based sensors, ACS Sens. 6 (2021) 1461–1481.
[44] Z. Wu, D. Nan, H. Yang, S. Pan, H. Liu, X. Hu, A ratiometric fluorescence-scattered light strategy based on MoS2 quantum dots/CoOOH nanoflakes system for ascorbic acid detection, Anal. Chim. Acta 1091 (2019) 59–68.
[45] F.L. Zu, F.Y. Yan, Z.J. Bai, J.X. Xu, Y.Y. Wang, Y.C. Huang, et al., The quenching of the fluorescence of carbon dots: a review on mechanisms and applications, Microchim. Acta 184 (2017) 1899–1914.
[46] S.S. Lu, S. Wang, J.H. Zhao, J. Sun, X.R. Yang, Fluorescence light-up biosensor for microRNA based on the distance-dependent photoinduced electron transfer, Anal. Chem. 89 (2017) 8429–8436.
[47] G. Li, H. Fu, X. Chen, P. Gong, G. Chen, L. Xia, et al., Facile and sensitive fluorescence sensing of alkaline phosphatase activity with photoluminescent carbon dots based on inner filter effect, Anal. Chem. 88 (2016) 2720–2726.
[48] Q. Hu, L. Gao, S.-q Rao, Z.-q Yang, T. Li, X. Gong, Nitrogen and chlorine dual-doped carbon nanodots for determination of curcumin in food matrix via inner filter effect, Food Chem. 280 (2019) 195–202.
[49] Y. Li, H. Wang, F. Dai, P. Li, X. Jin, Y. Huang, et al., Label-free fluorescent enzymatic assay of citrate synthase by CoA–Au(I) co-ordination polymer and its application in a multi-enzyme logic gate cascade, Biosens. Bioelectron. 86 (2016) 1038–1046.

Mengke Wang is an associate professor in the Key Laboratory for Medical Functional Nanomaterial of Jining Medical University, China. She received her doctor's degree from Jilin University (China) in 2021. Her research interests cover the synthesis the applications of fluorescent nanoprobes and nanozymes in biomedical sensing field.

Yaqing Han is currently carrying out her master's degree under the guidance of professor Guannan Wang in Jining Medical University (China). Her research focuses on the synthesis and application of metal nanoclusters for sensing.

Rui Huang is an associate professor at the School of Materials Science and Engineering, Hainan University (China). Her research is mainly focused on the synthesis of carbon dots@metal organic frameworks nanocomposites and their applications for biosensors.

Zhonghao Wang is a lecturer in the Key Laboratory for Medical Functional Nanomaterial of Jining Medical University, China. His research interests cover the synthesis and characterization of polymeric carbon nitride-based nanomaterials for photocatalysis and biomedical sensing.

Guannan Wang is currently a group leader and a full professor in School of Pharmacy of Shenyang Medical University; the part-time professor and honorary-director in the Key Laboratory for Medical Functional Nanomaterial of Jining Medical University, China. He received his Ph.D. in Analytical Chemistry from Jilin University, China, in 2011, as a postdoctoral researcher in 2012 under Pro Kajsa Uvdal in LinkÖping University. His research interests focus on bioactive materials, nanoprobes, and nanozymes used for bioengineering, nanocatalysis, and sensing activity.